Microsyst Technol (2012) 18:1297–1307
DOI 10.1007/s00542-012-1529-6

TECHNICAL PAPER

A new liquid crystal lens with axis-tunability via three sector electrodes

Tse-Yi Tu · Paul C.-P. Chao · Chin-Teng Lin

Received: 30 September 2011 / Accepted: 7 May 2012 / Published online: 30 May 2012

Abstract A novel liquid crystal (LC) lens with an on-line tunability on focus length and optical axis is proposed in this study. The designed lens has a LC layer sandwiched by two ITO glasses, one of which is patterned with three sector electrodes. With varied sets of pre-designed voltages applied to these three electrodes, the LC lens can not only render focusing effects but also tunability on the optical axis of the lens to an arbitrary axis. A vector-form equation is developed to predict the direction of axis tuning. Simulations are next conducted to predict dynamics of the LCs in the lens and also the focusing and axis-tuning properties of the lens. Important sizes and materials and fabrication process of the lens are determined and optimized based on simulation results. The designed LC lens is fabricated, and then experiments are conducted to demonstrate the performance of the designed LC lens on axis tuning. It shows that the focusing axis of the LC lens can be effectively changed by pre-calculated combinations of three voltages. It is also shown that the average movement of the focal point per applied voltage reaches 4.778 μm/V.

1 Introduction

Liquid crystal (LC) lenses have attracted many researchers in recent years (Sato 1979; Naumov et al. 1998) due to its on-line tunability on the focusing length. It could serve as a potential device in a phone camera to save the thickness of a conventional lens module. An LC lens is an optical lens having a structure of a LC material layer sandwiched by two glasses with the appropriate electrode patterns (Galstian et al. 2007; Ye et al. 2007). The focus length of an LC lens can be altered along the fixed axis by application of an external applied voltage. Furthermore, the electrical control of the focal length in a LC lens is more convenient and precise than mechanical control in a traditional variable-focus lens.

Over the past few years, there has been significant progress made in the study of LC lenses with electrically controllable focal lengths. Most studies paid efforts on the on-axis optical performance (Ye et al. 2004; Ren and Wu 2006; Ren et al. 2007). Only a few studies have so far investigated the phenomena of off-axis optics (Ye and Sato 2003; Ye et al. 2004, 2006a, b; Kirby et al. 2005); however, there is a lack of numerical analysis of this phenomenon. The purpose of this paper is to establish a practical numerical model of a tunable-axis LC lens for distilling the on-line tuning guidelines and then to verify the model experimentally.

The off-axis focusing of LC lenses with two and four electrodes were proposed in the past studies (Ye et al. 2006a, b; Fraval and Berier 2011). The maximum amount of focusing of LC lens which has bisection electrodes is 10.3 μm/V, but it shifts only in one direction. The LC lens with four electrodes easily focuses in the plane but it only shifts 4.16 μm/V. However, they could not develop an operative rule to control the degree in off-axis for focusing. Moreover, it is difficult to design the driver circuit when the LC lens has more electrodes. In this study, a novel LC lens is designed with three electrodes which are equally divided around 360° and shaped in sectors. A heuristic vector-form equation used to predict the level of

T.-Y. Tu · P. C.-P. Chao (✉) · C.-T. Lin
Department of Electrical Engineering,
National Chiao Tung University, Hsinchu, Taiwan, ROC
e-mail: pchao@mail.nctu.edu.tw

P. C.-P. Chao
Institute of Imaging and Biomedical Photonics,
National Chiao Tung University, Tainan, Taiwan, ROC

axis-tuning is established. The parameters involved in this equation are calibrated prior to the use for predicting and controlling the degree of axis tuning of focusing. Based on this vector equation, the desired electrode voltages can be solved for a given focusing axis. The designed LC lens is fabricated, and then experiments are conducted to demonstrate the performance of the designed LC lens on axis tuning. It shows that the focusing axis of the LC lens can be effectively changed by pre-calculated combinations of three voltages. The degree of axis-tuning conforms to those predicted by vector-form equations and simulations. It is also shown that the average movement of the focal point per applied voltage reaches 4.778 μm/V.

2 Lens design

2.1 Design principles

An LC lens is made from a layer of LC materials with the appropriate electrode structures. A conventional hole-type LC lens is designed to be equipped with a hole-patterned electrode at the top of the upper glasses, while a non-patterned planar ITO electrode on the lower glass, as illustrated in Fig. 1. This structure forms an electric field in a normal distribution which has the weakest electrical field intensity at the central region of the electrode's hole (i.e. aperture), as shown in Fig. 2. It causes un-uniformity of the electric field when a voltage crosses the two electrodes (Collings and Hird 1997; Lueder 2001). In the aperture region, the electric field is weaker near the center and strongest around the edge, as shown in Fig. 3a. Therefore, the refractive index in the aperture region is axisymmetric in distribution. The effects of the electric field and the distribution of the refractive index cause the incident light to focus, as shown in Fig. 3b (Barbero and Evangelista 1997; Yeh and Gu 1999; Hecht 2002). The difference in potential between the upper and bottom electrodes can affect the focal strength of the LC lens, which is the factor that can be used to control the LC lens. However, various sizes of lens aperture are required for the camera module for cell phone applications; therefore, three different sizes of LC lens apertures are fabricated and measured for the present study. The measurement results of the effective focal length of the LC lens is shown in Fig. 4. When the voltage of the upper electrode of the LC lens is increased, the effective focal length (EFL) of the LC lens becomes shorter. According to the experimental result, there is the largest change in the EFL when the aperture of the LC lens is 3 mm. The least EFL for the 3 mm hole type LC lens is 118.57 mm; the potential of the upper electrode is 80 V. In fact, the LC lens has the ability to change the EFL by applying different voltages.

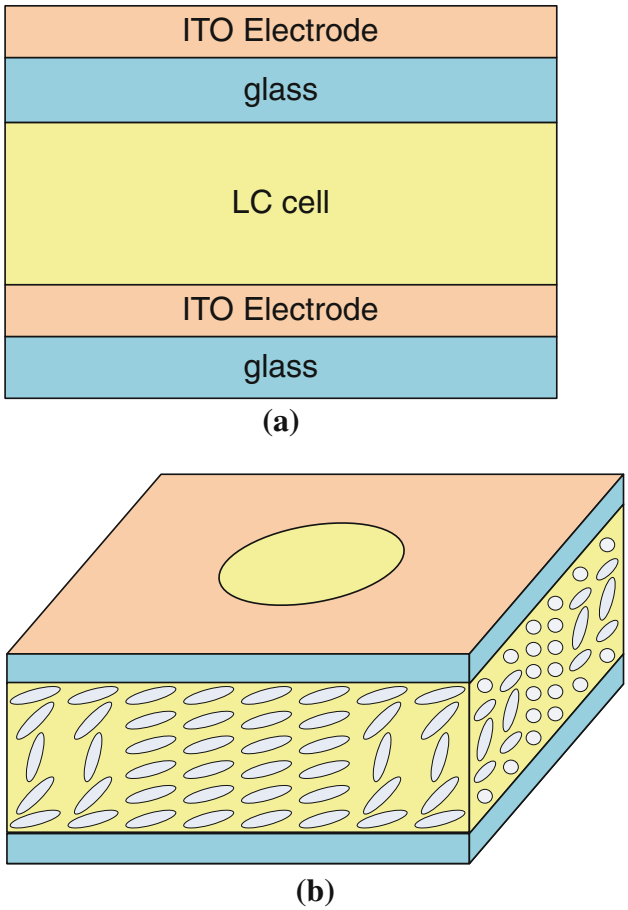

Fig. 1 **a** Material layers of the LC lens; **b** the hole-type LC lens

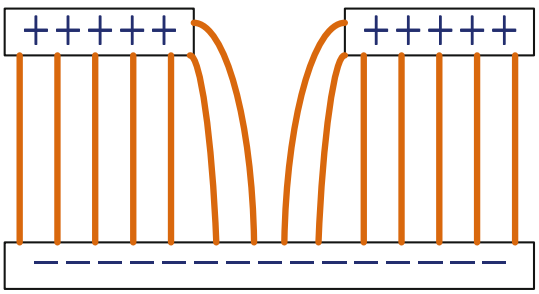

Fig. 2 Potential lines of the hole-type LC lens

2.2 Design with two electrodes

The hole-type LC lens can be transformed into a simple tunable LC by dividing the upper electrode of the hole-type LC lens into two parts. The structure of this two-electrode LC lens is shown in Fig. 5. The potential of the right and left electrodes are designated by V_R and V_L, respectively. When V_R is not equal to V_L, the LC lens has a symmetrical and un-uniform electric field which causes one dimension off-axis focusing. With the simple design in hand, this two-electrode LC lens is fabricated in a laboratory. Experiments are conducted to verify the performance. The measured

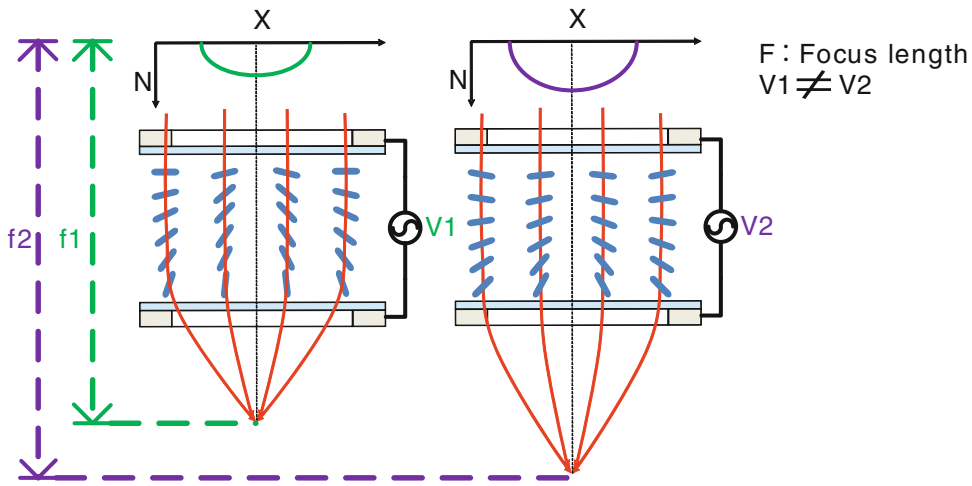

Fig. 3 Variable focusing of the LC lens

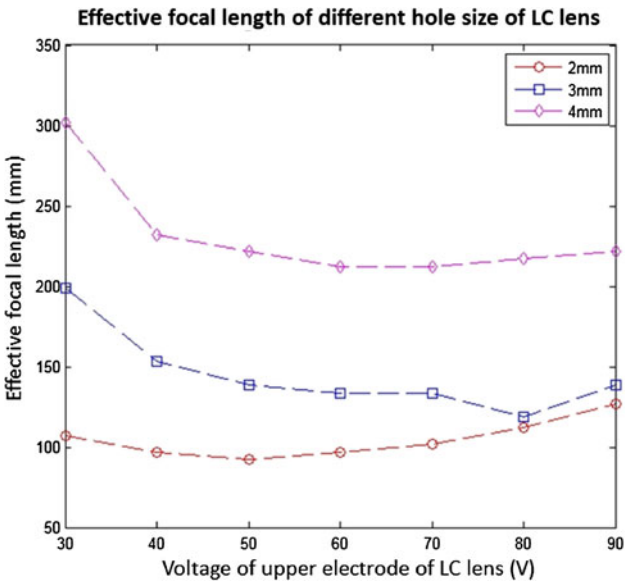

Fig. 4 The effective focal length of the LC lens

interference patterns of this two-electrode LC lens are shown in Fig. 6. There is a distinct change in pattern when V_L voltage decreases. Figure 7 shows the focusing position extracted from the figures in Fig. 6. In the experiment, V_R is constant and V_L is varied in experiment. It is seen that the focal point shifts toward the electrode with the lower potential (the left electrode). The focal point initially follows a straight horizontal line but diverge to un-expected values, which in fact lost the capability of focusing. The is probably due to a large difference between the two electrode voltage that deteriorates the original function of focusing by the LC lens. The tilt angle of the optical axis of the two electrodes to which voltages of 80 and 60 V are applied on V_R and V_L is 0.045°, as see in Table 1. However, the shift in focusing axis is restricted to one dimension.

2.3 Design with three electrodes

The structure of the three-electrode LC lens is shown in Fig. 8. The upper electrode is divided the three sub-electrodes that form 120° sectors individually. The three sub-electrodes are designated as E_I, E_{II}, and E_{III}. The symmetrical axes of E_I, E_{II}, and E_{III} intersect each other at 120°, an advantage for controlling the focus point. Three is the least number of electrodes needed to control shifting of the focal point on the focal plane based on simple heuristic vector theorem. The simulation of the electric field of the LC lens is shown in Fig. 9 (Ge et al. 2005). The voltages applied to E_I was 80, 75, 70, 65, and 60 V and the potential of E_{II} and E_{III} is 80 V. When E_I, E_{II}, and E_{III} have the same potential, the equipotential lines appear as concentric circles. When different potentials are applied to E_I, E_{II}, and E_{III}, the equipotential lines incline toward the direction of the sub-electrode with the higher potential, showing the capability of axis tuning.

It is interesting at this point to establish a heuristic equation to control the focusing axis of the tunable-axis LC lens. To this end, an LC lens with three sector electrodes in i–j vector coordinates is considered, as shown in Fig. 10a. The lens is assumed responsible for imaging at a given plane with a distance from the lens as the focal length, denoted by FL. Figure 10b illustrates the corresponding geometry. The focusing position of the tunable-axis LC lens at the focal plane is assumed heuristically as a vector-form function of the three voltages applied to three sub-electrodes, that is,

$$\begin{aligned}\vec{P}_F &= \alpha(V_{II}\sin 60 - V_{III}\sin 60)\vec{i} \\ &\quad + \beta(V_I - V_{II}\cos 60 - V_{III}\cos 60)\vec{j} \\ &= \frac{\sqrt{3}}{2}\alpha(V_{II} - V_{III})\vec{i} + \frac{1}{2}\beta(2V_I - V_{II} - V_{III})\vec{j}\end{aligned} \quad (1)$$

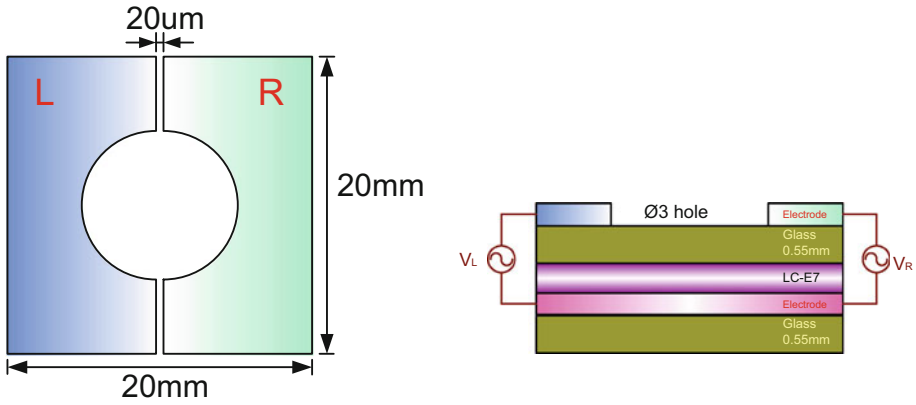

Fig. 5 The structure of the LC lens with two electrodes

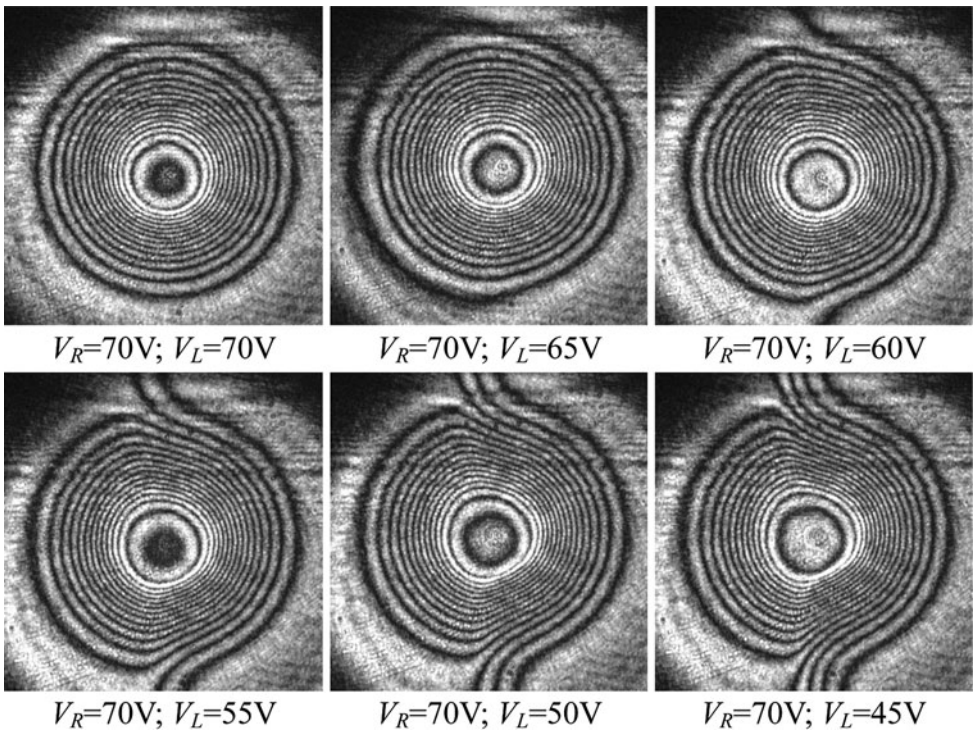

Fig. 6 Interference pattern of the LC lens with two electrodes

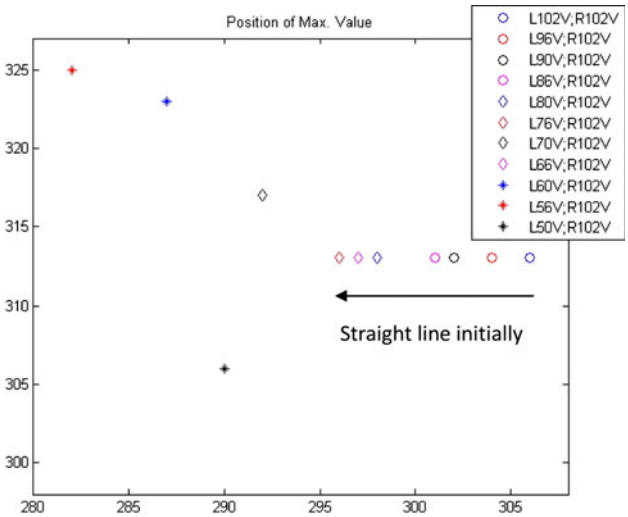

Fig. 7 Focus shifting of the LC lens with two electrodes

where V_I, V_{II}, and V_{III} are the voltages applied to electrodes E_I, E_{II}, and E_{III}, respectively; α and β are the parameters to identified based on experimental data. Note that the predicted position of focal point $\vec{P}_F$ at the focal plane also reflects the tilting angle of the optical axis of the designed LC lens, which based on simple geometry, can be derived by

Table 1 Tilting angle of the optical axis by the LC lens with two electrodes

Left voltage (V_L)	Right voltage (V_R)	Focus length (mm)	Optical-axis tilting angle (°)
80	80	97	0
80	60	103	0.045
60	60	113	0

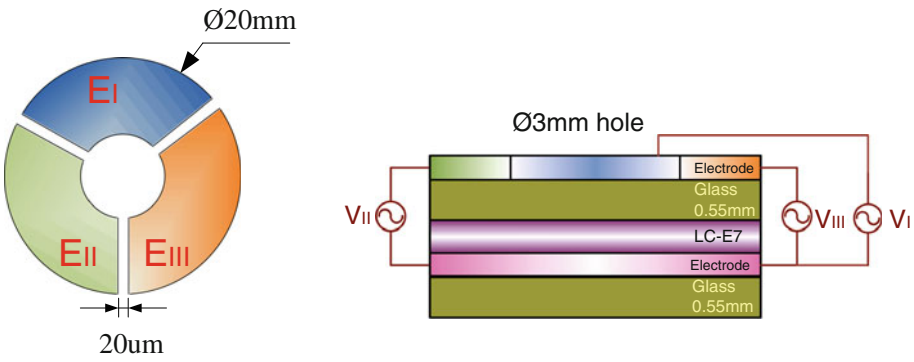

Fig. 8 The structure of the LC lens with three sub-electrodes

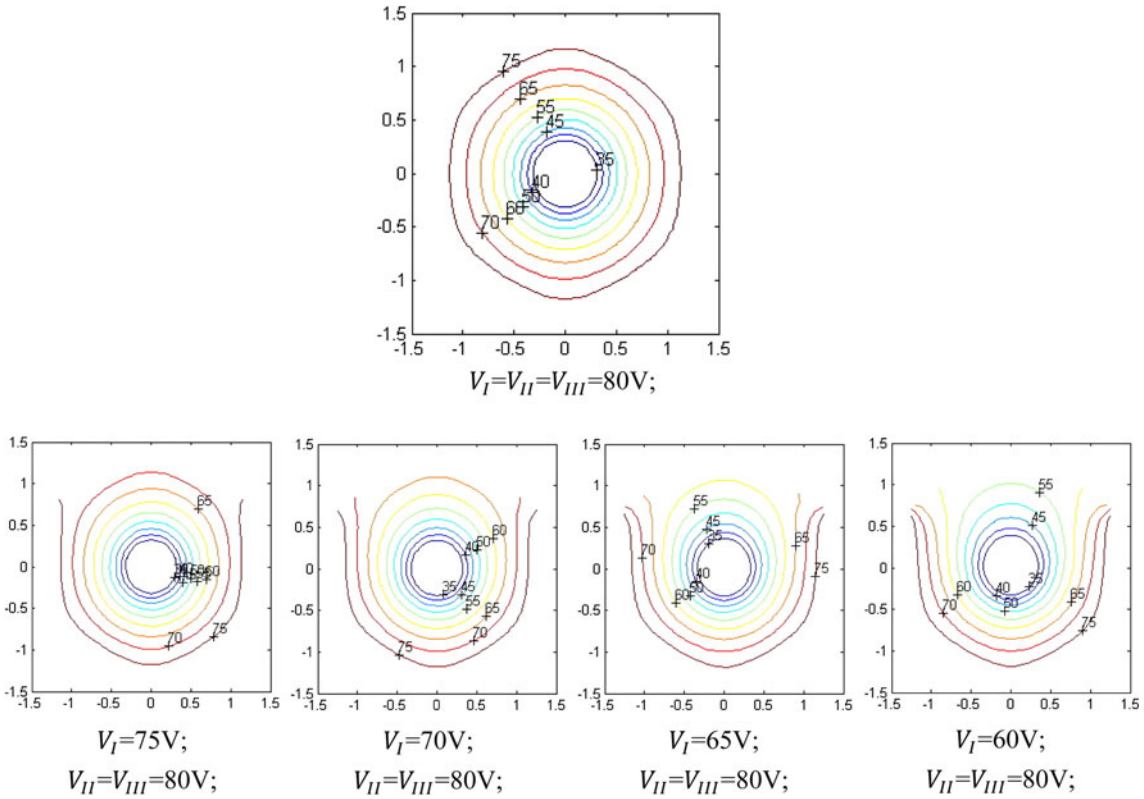

Fig. 9 Equipotential lines of the LC lens

$$\theta = \tan^{-1}\frac{|\vec{P}_F|}{FL} \tag{2}$$

Note that the derivation of the tilting angle via the above equation needs assistance from available measured focal lengths and [α, β] identified from experimental data.

3 Fabrication

The fabrication process of the LC lens consists of two primary procedures. One involves indium tin oxide (ITO) electrode etching and the other is alignment to the ITO surface. The quality of the ITO electrode influences the electric field and the character of alignment influences the LC's pretilt angle. The ITO electrode etching fabrication process is shown in Fig. 11. The ITO glass is from Applied Vacuum Coating Technologies Co., Ltd. (AVCT). The thickness of the ITO glass is 0.55 mm and it is 30–40 μm. This ITO glass is characterized by high transmission of about 94 % conforms to the quality needed for the LC Lens. The primary fabrication procedure is outlined below.

1. *Cleaning* The ITO glass must be cleaned and dried before starting the ITO etching process.
2. *Coating of the photo resist* The specifications for the AZ-300 photo resist used are given in Table 2. The ITO glass is placed on the spin coating machine and

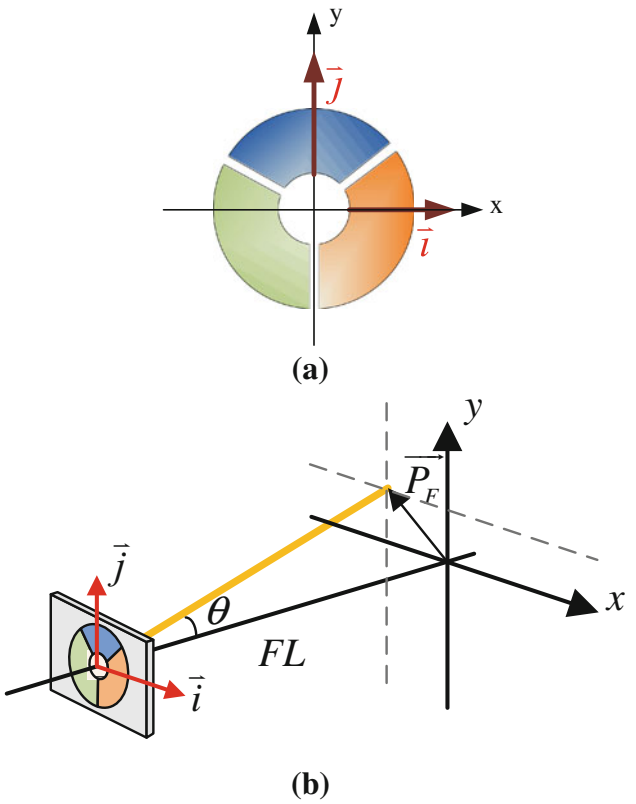

Fig. 10 **a** Three sector electrodes of the designed tunable-axis LC lens; **b** geometry of focusing

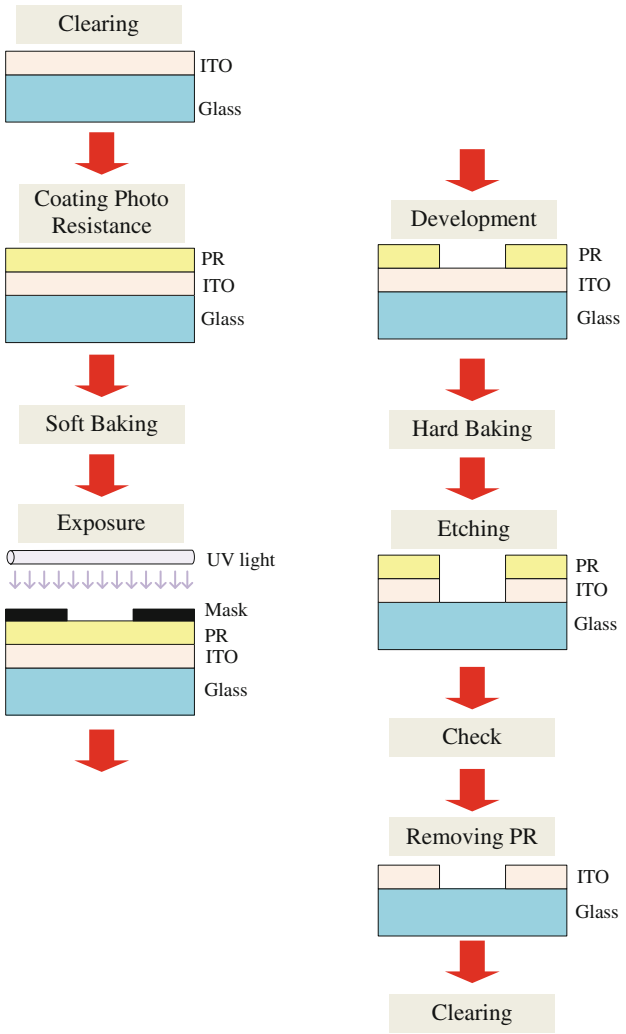

Fig. 11 Fabrication procedure of etching ITO electrode

the photo resist poured onto the center of the ITO glass. The spin speed is set at 420 rpm for 30 s.

3. *Pre-baking* At 100 °C for 15–30 min.
4. *Exposure* The mask for creating the ITO electrode pattern on the ITO glass is placed in the UV exposure machine. The exposure time is set for 200 s.
5. *Development* The ITO glass is then immersed in the developing solution in the AZ-300 Developer for a few seconds. The exposed ITO is dissolved in developing solution.
6. *Hard baking* At 120 °C for 30 min.
7. *ITO etching* The etching solution is prepared using the formula, HCL:HNO_3:H_2O = 47:3:50, by volume. The ITO glass is immersed in the etching solution at 12,350 °C. The etching area is checked to see if it is without the ITO, like the center of the hole type LC lens.
8. *Removal of the photo resist* The ITO glass is immersed in acetone to remove the photo resist. After hard baking the photo resist is not removed by the developer therefore acetone is used to remove it and the other chemical reagent.
9. *Cleaning and drying* Detergent, water, and methanol are placed into the ultra-sound machine. The ITO glass is cleaned by being immersed in the solution in sequence and finally dried.

On the other hand, Fig. 12 shows the procedure for alignment on the ITO surface. The primary steps are outlined as follows:

1. *Polyimide coating* A spin coating machine, set at 5,000 rpm for 30 s is used to spread the polyimide onto the ITO glass. The polyimide used is AL-1426B from Daily-Polymer Corp. From the specified, the pretilt angle is 2°.
2. *Hard baking* At 185 °C for 1 h.
3. *Rubbing* A rubbing machine rubs the microgrooves on the PI surface of the ITO glass. The micro-grooved surface provides the surface for anchoring the LC to the ITO glass surface.

With ITO glasses etched and the alignment PI layer rubbed, the LC lens is assembled. In the assembling

Table 2 Sample process conditions for AZ-300

Pre-baking	100 °C 90 s
Exposure	FPD Exposure tools
Developing	KOH solution 1.0 wt% 23 °C 60 s
	AZ 300MIF (2.38 %) 23 °C 60 s
Rinsing	DI-water 30 s
Post-baking	120 °C 90 s (DHP) and/or 15–30 min (Oven)
Stripping	AZ remover high density alkali solution

process, the Newton's ring interference pattern is checked to determine whether the ITO electrodes are parallel or not. The following steps are used for packaging:

1. The spacer is placed onto the fringe of the substratum of the ITO glass.
2. UV adhesive is smeared on the edge of the ITO glass spacer.
3. The upper ITO glass is placed so as to cover the substratum ITO glass.
4. The Newton's ring is used to check whether the two pieces of glass are parallel and adjustments made given the pattern in the central region.
5. The adhesive is cured by UV light.

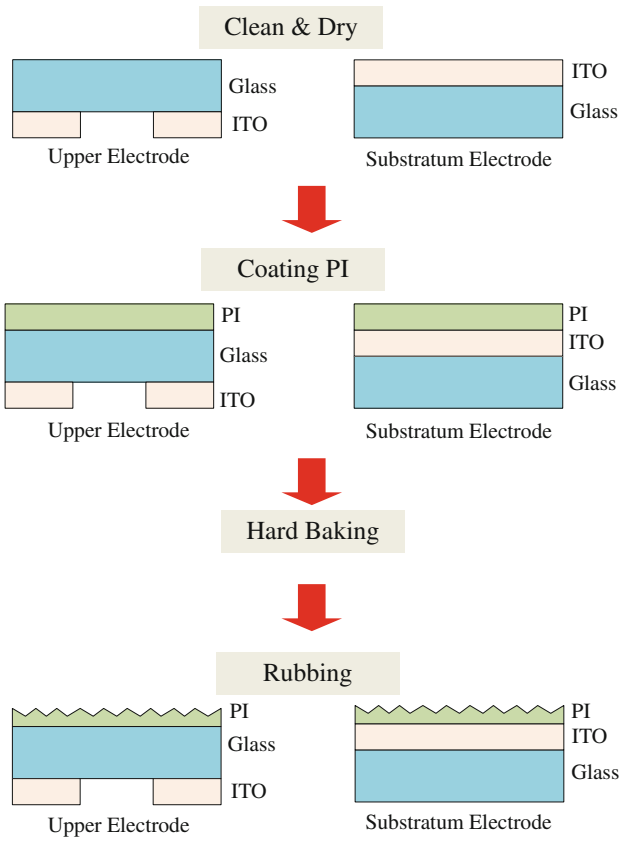

Fig. 12 The ITO alignment process

Table 3 Optical properties of E7 (wavelength at 633 nm)

Parameters	Value (unit)
Refractive index of *e-ray*	1.7371
Refractive index of *o-ray*	1.5183
Optical anisotropy, Δn	0.2188
Elastic constants, K_{11}	11.1 pN
Elastic constants, K_{22}	5.9 pN
Elastic constants, K_{33}	17.1 pN
Dielectric constants parallel to the director, $\varepsilon_{\parallel}$	19.28
Dielectric constants perpendicular to the director, $\varepsilon_{\perp}$	5.21
Rotational viscosity, γ	233 m Pa sec

6. The upper and substratum ITO glass is combined to form a package.

After this the LC is injected into the gap between the upper and substratum ITO glass layers. The E7 LC obtained from Merck has an ordinary refractive index n_o, of 1.5183 and an extraordinary refractive index n_e of 1.7371. The specifications for E7 are shown in Table 3. After injecting the LC, the two rims of the ITO glass layers without the spacer package are fastened by UV adhesive and cured.

Finally, the wires are linked to the two electrodes by sliver adhesive and tinning-copper foil tapes. The conduction of the wires with two electrodes is checked. A picture of the LC lens is shown Fig. 13.

4 Experimental validation

The experimental setup is shown in Fig. 14. A laser beam analyzer is utilized to catch the movement of focus in order to measure the phenomenon of the tunable-axis LC lens. The Ophire FX-50 laser beam analyzer can record the power in each 10 μm square of the measure plane. It can measure a rectangular region 6.4× 4.8 mm in size. A He–Ne laser beam polarized in the rubbing direction of LC lens is normally incident on the LC lens. The LC lens is driven by AC voltage, 1 KHz frequency. The laser beam analyzer is placed in the focal plane to observe the laser spot. The focal length is first detected by moving the image plane along the optical axis to the position where the focal spot is in its smallest size with the highest energy density. With three electrode voltages set as 80 V, the focal length is found as 201 mm.

For subsequent experimental study, two different levels of voltage are applied to the electrodes of the LC lens for each case of experimental trials, V_H and V_L, via the three separate electrodes. To simplify the complexity of the experiments, the same voltage, either V_H or V_L is applied to

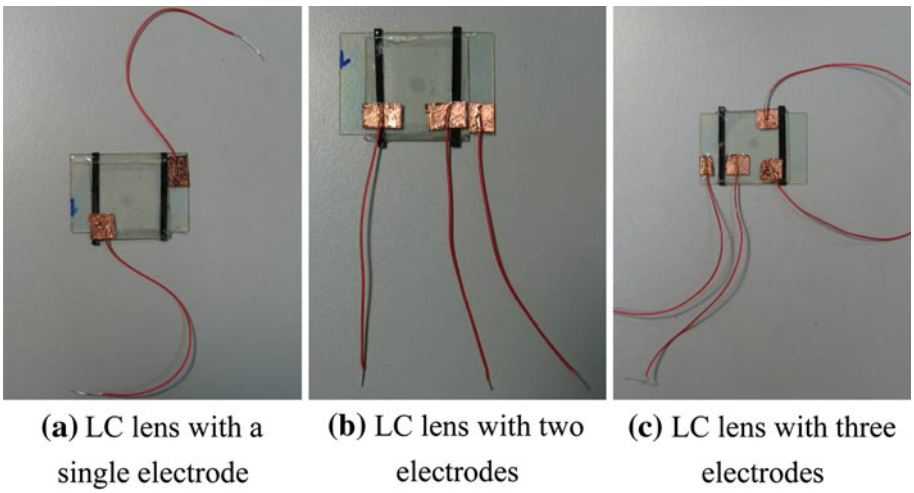

Fig. 13 Samples of the LC lens

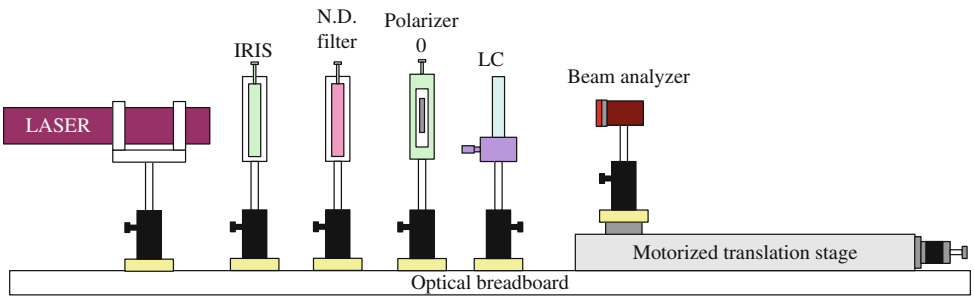

Fig. 14 Measurement system with the laser and the beam analyzer: **a** schematic; **b** experimental apparatus

two of the sub-electrodes. V_H is the high potential voltage and it is fixed at a constant voltage of 80 V; while V_L is the low potential voltage and is varied: 75, 70, 65, and 60 V. V_I is the potential on electrode E_I; V_{II} is the potential of E_{II}; and V_{III} is the potential of E_{III}. A laser beam analyzer (Ophire PX-50) is used to observe the movement of the optical axis, or the focal point on the observing plane. The analyzer is placed on the optical path at a distanced from the LC lens of 201 mm, the focal length measured previously.

Figure 15 plots the experimental locations of the focal point detected by the beam analyzer with different combinations of applied voltages. With the measured focal points available, the focal point is also predicted using Eq. (1) with the values of α and β identified based on all sets of experimental focal point locations. In this identification process, each measured focal point location is used to reversely calculate the parameter values of α and β. The final adopted values of α and β are averages of all calculated α and β, resulting in that α is 3.34 and β is -2.783.

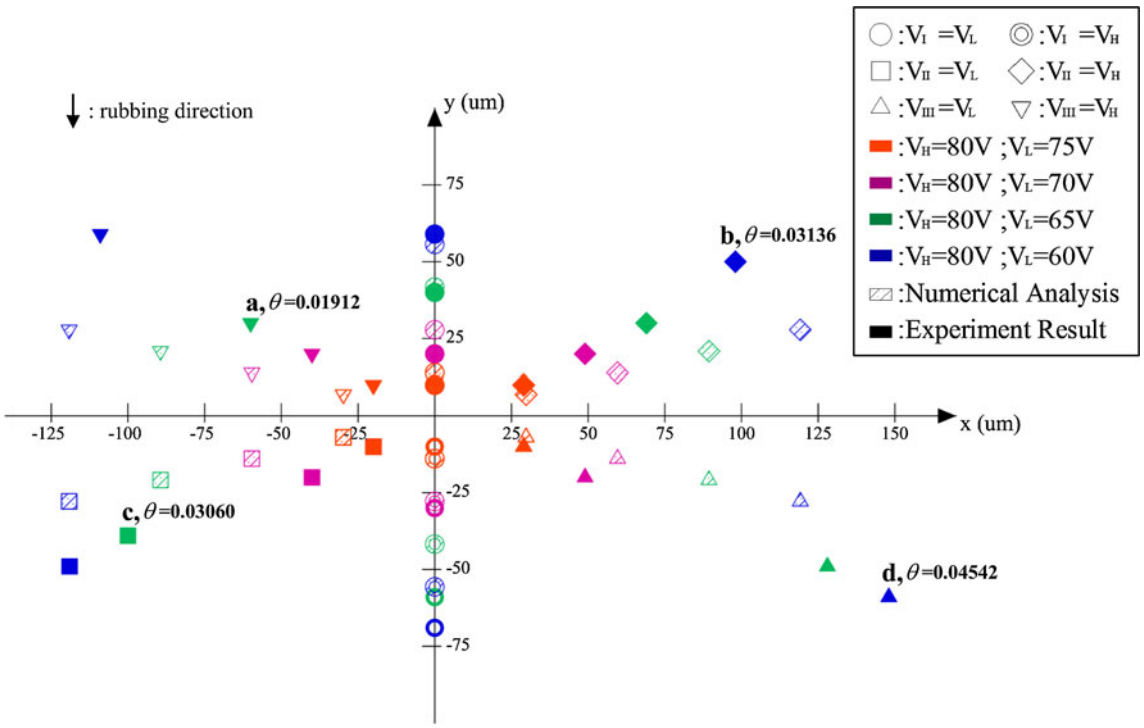

Fig. 15 Focus spots on the focal plane

Table 4 Results of axis tuning for the LC lens with three sub-electrodes

$V_H - V_L$	V_I	V_{II}	V_{III}	Δx (μm)	Δy (μm)	Optical-axis tilt angle (°)
5	75	80	80	0	10	0.00285
	80	75	80	−20	−10	0.00637
	80	80	75	29	−10	0.00874
	80	75	75	0	−10	0.00285
	75	80	75	29	10	0.00874
	75	75	80	−20	10	0.00637
10	70	80	80	0	20	0.00570
	80	70	80	−40	−20	0.01275
	80	80	70	49	−20	0.01509
	80	70	70	0	−30	0.00855
	70	80	70	49	20	0.01509
	70	70	80	−40	20	0.01275
15	65	80	80	0	40	0.01140
	80	65	80	−100	−39	0.03060
	80	80	65	128	−49	0.03907
	80	65	65	0	−59	0.01682
	65	80	65	69	30	0.02145
	65	65	80	−60	30	0.01912
20	60	80	80	0	59	0.01682
	80	60	80	−119	−49	0.03668
	80	80	60	148	−59	0.04542
	80	60	60	0	−69	0.01967
	60	80	60	98	50	0.03136
	60	60	80	−109	59	0.03533

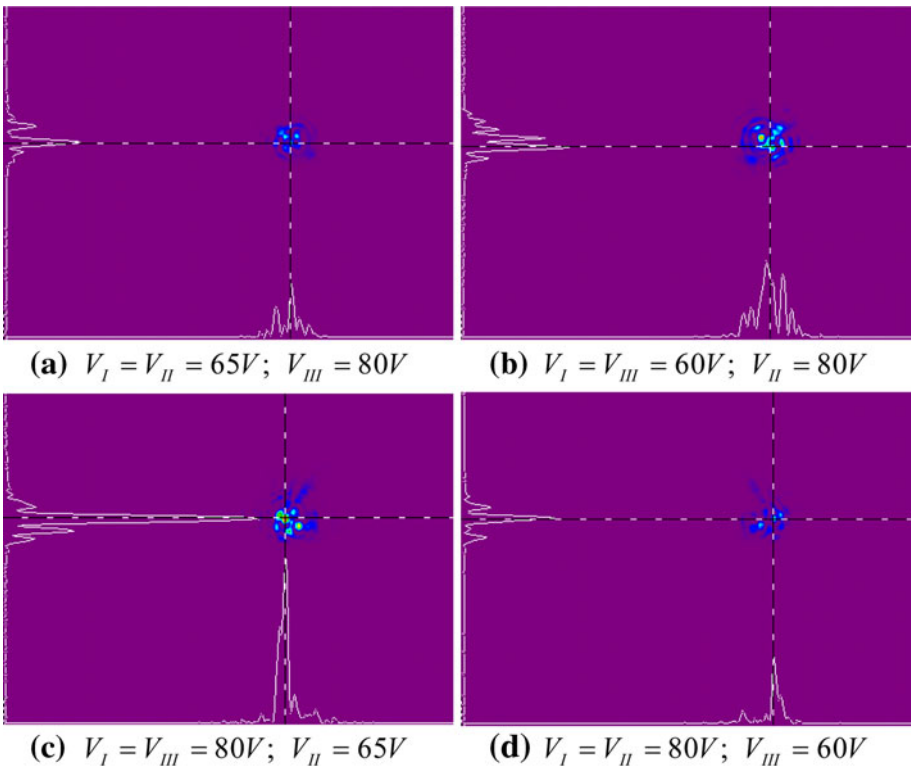

Fig. 16 Beam profiles detected by the analyzer

In Fig. 15, the symbols in different colors correspond to three different types of operation, where the difference between V_H and V_L varies from low to high. On the other hand, solid symbols correspond to experimental data, while the symbols filled with oblique lines correspond to the numerical data predicted by Eq. (1). The movements of the focal point in number for those data in Fig. 15 are listed in Table 4. Based on these data, the average movement of the focal point per applied voltage reaches 4.778 μm/V, which is commensurate with the results reported in (Ye et al. 2006a, b) based on simple extra conversions.

Four beam profiles detected by the analyzer are selected for demonstration in Fig. 16. These four profiles correspond to the four furthest focal points as denoted in Fig. 15 with tilting angle calculated by Eq. (2). The largest tilting angle of the optical axis is 0.04542°. Various aspects of axis-tuning capability offered by the designed LC lens are demonstrated by the data in Fig. 15, as stated in the followings.

(1) When the control voltages follow that $V_I = V_L$ and $V_{II} = V_{III} = V_H$, or $V_I = V_H$, and $V_{II} = V_{III} = V_L$, the focal point moves along the y axis which is the symmetrical axis of E_I as shown in Fig. 15. The predicted focal points are seen close to their experimental counterparts, showing the effectiveness of Eq. (1) to predicting the tilting angle the optical axis for the designed LC lens. However, the difference between the focal points resulted from experiment and their counterpart predicted by Eq. (1) becomes larger as tilting angle is increased. The corresponding largest difference in tilting angle [calculated by Eq. (2)] is in a moderate level of 0.04919°.

(2) When the control voltages follow that $V_{II} = V_L$ and $V_I = V_{III} = V_H$, or $V_{II} = V_H$ and $V_I = V_{III} = V_L$, the focal point moves approximately along the 30° and −150° axes which are the symmetrical axes to E_{II}, as shown in Fig. 15. The predicted focal points are seen much away from their experimental counterparts as tilting angle of the optical axis increases, but in reasonable differences. The differences between experiments and predictions, different from the previous case 1, involve those in tilting level and direction.

(3) When the control voltage follow that $V_{III} = V_L$ and $V_I = V_{II} = V_H$, or $V_{III} = V_H$ and $V_I = V_{II} = V_L$, the focal point moves along the 150° and −30° axes, which are the symmetrical axis to E_{III}, as shown in Fig. 15. The predicted focal points are seen much away from their experimental counterparts as tilting angle of the optical axis increases, but in reasonable differences. The differences between experiments and predictions, different from the previous case 1, involve those in tilting level and direction.

5 Conclusion

A novel LC lens structure with three equally-divided sector electrodes is proposed, and the analysis of the electrical

potential field and experiments are carried out to verify the concept and design. The axis-tuning is made possible via applying different voltages to the three equally-divided sector electrodes. A vector-form equation is successfully developed to predict the direction and level of axis tuning. Simulations are also conducted on the electrical field generated by three sector electrode with applied voltages and then determine critical sizes of the LC lens. The designed LC lens are thus successfully fabricated and tested in experiments. It is found from the experimental results that the prediction equation established is able to predict the level of axis-tilting within reasonable errors. The average movement of the focal point per applied voltage reaches 4.778 μm/V. The present study shows that both simulation and experiments validate the effectiveness of the sector electrode design and the prediction via the established vector-form equation for axis tuning.

Acknowledgments The authors appreciate the support from National Science Council of R.O.C under the grant no. NSC 101-2623-E-009-006-D and 100-2221-E-009-091-. This work was also supported in part by the UST-UCSD International Center of Excellence in Advanced Bio-Engineering sponsored by the Taiwan National Science Council I-RiCE Program under Grant NSC-100-2911-I-009-101.

References

Barbero G, Evangelista LR (1997) An elementary course on the continuum theory for nematic liquid crystals, World Scientific

Collings PJ, Hird M (1997) Introduction to liquid crystals, Taylor & Francis, UK

Fraval N, Berier F (2011) Liquid crystal lens auto-focus extended to optical image stabilization for wafer level camera Proc. of SPIE 7930:793009-1–793009-8

Galstian T, Presniakov V, Asatryan K, Tork A (2007) Electrically variable focus polymer-stabilized liquid crystal lens having non-homogenous polymerization of a nematic liquid crystal/monomer mixture United States Patent, US 7218375

Ge Z, Wu TX, Lu R, Zhu X, Hong Q, Wu S-T (2005) Comprehensive three-dimensional dynamic modeling of liquid crystal devices using finite element method. J Disp Technol 1(2):194–206

Hecht E (2002) Optics, Addison Wesley, Boston

Kirby AK, Hands PJW, Love GD (2005) Optical design of liquid crystal lenses: off-axis modeling. Proc SPIE Int Soc for Opt Eng 1:1–10

Lueder E (2001) liquid crystal displays addressing schemes and electro-optical effects, John Wiley Ltd., London

Naumov AF, Loktev MYu, Guralnik IR, Vdovin G (1998) Liquid-crystal adaptive lenses with modal control. Opt Lett 23(13): 992–994

Ren H, Wu S-T (2006) Adaptive liquid crystal lens with large focal length tunability. Opt Express 14(23):11292–11298

Ren H, Fox DW, Wu B, Wu S-T (2007) Liquid crystal lens with large focal length tunability and low operating voltage. Opt Express 15(18):11328–11335

Sato S (1979) Liquid-crystal lens-cells with variable focal length. Jpn J Appl Phys 18(9):1679–1684

Ye M, Sato S (2003) Liquid crystal lens with focus movable along and off axis. Opt Commun 225:277–280

Ye M, Wang B, Sato S (2004) Liquid-crystal lens with a focal length that is variable in a wide range. Appl Opt 43(35):6407–6412

Ye M, Wang B, Sato S (2006a) Liquid crystal lens with focus movable in focal plane. Opt Commun 259:710–722

Ye M, Wang B, Sato S (2006b) Study of liquid crystal lens with focus movable in focal plane by wave front analysis. Jpn J Appl Phys 45(8A):6320–6322

Ye M, Wang B, Sato S (2007) Development of high quality liquid crystal lens. Proc. of SPIE 6487:64870N-1–64870N-12

Yeh P, Gu C (1999) Optical of Liquid Crystal Displays John Wiley Inc., London